Anal Bioanal Chem (2013) 405:3137–3151
DOI 10.1007/s00216-013-6759-7

ORIGINAL PAPER

Comparative study of recent wide-pore materials of different stationary phase morphology, applied for the reversed-phase analysis of recombinant monoclonal antibodies

Szabolcs Fekete · Jean-Luc Veuthey · Sebastiaan Eeltink · Davy Guillarme

Received: 3 October 2012 / Revised: 11 January 2013 / Accepted: 16 January 2013 / Published online: 29 January 2013

Abstract Various recent wide-pore reversed-phase stationary phases were studied for the analysis of intact monoclonal antibodies (mAbs) of 150 kDa and their fragments possessing sizes between 25 and 50 kDa. Different types of column technology were evaluated, namely, a prototype silica-based inorganic monolith containing mesopores of ~250 Å and macropores of ~1.1 μm, a column packed with 3.6 μm wide-pore core-shell particles possessing a wide pore size distribution with an average around 200 Å and a column packed with fully porous 1.7 μm particles having pore size of ~300 Å. The performance of these wide-pore materials was compared with that of a poly(styrene–divinyl benzene) organic monolithic column, with a macropore size of approximately 1 μm but without mesopores (stagnant pores). A systematic investigation was carried out using model IgG1 and IgG2 mAbs, namely rituximab, panitumumab, and bevacizumab. Firstly, the recoveries of intact and reduced mAbs were compared on the two monolithic phases, and it appeared that adsorption was less pronounced on the organic monolith, probably due to the difference in chemistry (C18 versus phenyl) and the absence of mesopores (stagnant zones). Secondly, the kinetic performance was investigated in gradient elution mode for all columns. For this purpose, peak capacities *per* meter as well as peak capacities *per* time unit and *per* pressure unit (PPT) were calculated at various flow rates, to compare performance of columns with different dimensions. In terms of peak capacity *per* meter, the core-shell 3.6 μm and fully porous 1.7 μm columns outperformed the two monolithic phases, at a temperature of 60 °C. However, when considering the PPT values, the core-shell 3.6 μm column remained the best phase while the prototype silica-based monoliths became very interesting, mostly due to a very high permeability compared with the organic monolith. Therefore, these core-shell and silica-based monolith provided the fastest achievable separation. Finally, at the maximal working temperature of each column, the core-shell 3.6 μm column was far better than the other one, because it is the only one stable up to 90 °C. Lastly, the loading capacity was also measured on these four different phases. It appeared that the organic monolith was the less interesting and rapidly overloaded, due to the absence of mesopores. On the other hand, the loading capacity of prototype silica-based monolith was indeed reasonable.

Keywords Monolith · Core-shell · Sub-2 μm · Column efficiency · Monoclonal antibody

Introduction

In reversed-phase liquid chromatography (RPLC), there have been a significant number of innovations in terms of instrumentations and column technology during the last decade. The goal of these new technologies was to perform either faster analysis or to attain higher resolution. These advances have mainly been driven by the constant increase in the number of analyses or in sample complexity. These innovative strategies were generally developed for small molecules, but nowadays, RPLC also becomes a relevant strategy for the analysis of large biomolecules, such as therapeutic peptides, proteins, or monoclonal antibodies.

S. Fekete (✉) · J.-L. Veuthey · D. Guillarme
School of Pharmaceutical Sciences, University of Geneva, University of Lausanne, Bd d'Yvoy 20, 1211 Geneva 4, Switzerland
e-mail: szabolcs.fekete@unige.ch

S. Fekete
e-mail: szfekete@mail.bme.hu

S. Eeltink
Department of Chemical Engineering, Vrije Universiteit Brussel, Pleinlaan 2, 1050 14 Brussels, Belgium

Indeed, size exclusion chromatography and ion exchange chromatography are considered as reference techniques for analyzing such biomolecules but suffer from low kinetic performance and difficult coupling with mass spectrometry. Since high-molecular-weight proteins have large hydrodynamic radii, wide-pore RPLC stationary phases are mandatory for the analysis of mAbs and their fragments. There are now several novel RPLC stationary phases, commercially available with wide pores (200–300 Å at least).

Monolithic stationary phases are promising materials to improve chromatographic performance [1, 2]. They have originally been developed by Hjerten [3], Svec and Frechet [4], and Tanaka and Nakanishi [5] during the 1990s. Various types of inorganic (e.g., silica, zirconia, carbon, titania) or organic (e.g., polymethacrylate, polyacrylamide, poly(styrene–divinylbenzene) monoliths can be prepared but only polymethacrylate, poly(styrene–divinylbenzene), and silica-based monoliths are commercially available. The organic monoliths are generally applied for the separations of biomolecules, including oligonucleotides, peptides, and intact proteins including protein isoforms [6, 7]. On the other hand, silica-based monoliths are well adapted for the separation of small molecules, particularly since the introduction of the second generation of monoliths in 2011. The latter possesses macropores of 1.2 μm and mesopores of 15 nm. As recently reported [8], because of a more dense packing, this second generation of silica monoliths provides kinetic performance close to that of columns packed with porous sub-2 μm particles but with a reduced backpressure. In the case of large molecules, wide-pore silica-based monoliths are, however, not yet commercially available.

An alternative to monoliths is the use of columns packed with fully porous sub-2 μm particles. It is well established since the theoretical works of Giddings, Knox, and Poppe in the 1970s that small particles result in simultaneous improvement of efficiency, optimum velocity, and mass transfer [9–11]. However, the proof of concept of ultra-high-pressure liquid chromatography (UHPLC) was only demonstrated in 1997 by Jorgenson et al. [12, 13], and commercial systems and columns adapted to these high pressures became available in 2004 [14, 15]. Currently, several UHPLC instruments compatible with pressures up to 1,000–1,300 bar and numerous column chemistries and dimensions have become available (>10 providers and >80 chemistries) [16, 17]. It is also important to notice that columns packed with wide-pore porous sub-2 μm particles are now available from various providers, and a few UHPLC applications for large biomolecules have ever been reported [18–20].

Another possible strategy to improve throughput and/or resolution in liquid chromatography (LC) is the use of core-shell technology [21–23]. Basically, this approach consists of using superficially porous particles composed of a solid inner core surrounded by a porous outer shell. This technology has been originally developed by Kirkland in the 1990s and commercialized under the trademark Agilent Poroshell, to reduce the diffusion path that macromolecules travel [24]. Today, this strategy is mostly employed with 2.6–2.7 μm particles for analyzing small molecules, as it permits achieving equivalent performance to sub-2 μm particles but with a two- to threefold lower pressure [25–27]. A few applications demonstrated the interest of such technology for analyzing peptides and intact proteins [28]. More recently, some wide-pore core-shell particles became commercially available allowing the analysis of large proteins or even intact mAbs [29].

The goal of the present study was to investigate the possibilities and limitations of four different innovative wide-pore column technologies in RPLC, for the analysis of intact mAbs and their fragments. Two types of monoliths were tested, namely a prototype inorganic silica-based monolith and a poly(styrene/divinyl benzene) (PS-DVB) organic monolith. The performance was compared with that of a column packed with 3.6 μm core-shell particles possessing a wide pore size distribution (average pore size of ~200 Å) and that of a fully porous 1.7 μm particles, with pore size of ~300 Å. This work focuses on adsorption/recovery of mAbs, kinetic performance with large biomolecules, and loading capacity of the different materials.

Experimental

Chemicals, columns

Acetonitrile (gradient grade) was purchased from Sigma-Aldrich (Buchs, Switzerland). Water was obtained with a Milli-Q Purification System from Millipore (Bedford, MA, USA).

IgG monoclonal antibodies including rituximab (MabThera) and bevacizumab (Avastin) were purchased from Roche (Roche Pharma, Switzerland), and panitumumab (Vectibix) was purchased from Amgen (Switzerland). For fragmentation of the monoclonal antibodies, dithiothreitol (DTT) and papain (from *Carica* papaya) were obtained from Sigma-Aldrich (Buchs, Switzerland). Trifluoroacetic acid (TFA) and hydrochloric acid were purchased from Sigma–Aldrich (Buchs, Switzerland).

Acquity BEH-300 C18 column (150×2.1 mm, 300 Å) with a particle size of 1.7 μm (ethylene-bridged hybrid, BEH) was purchased from Waters (Milford, MA, USA). BEH technology particles are prepared from two monomers: tetraethoxysilane and bis(triethoxysilyl)ethane which incorporates the pre-formed ethylene bridges. The high degree of cross-linking ensures strong mechanical and hydrolytic stability. Moreover, the amount of residual silanols is significantly lower than it is on pure silica-based materials and therefore the silanol activity of this BEH phases is low compared with silica-based phases.

Aeris Widepore (WP) C18 column (150×2.1 mm) packed with 3.6 μm core-shell particles (silica) was purchased from Phenomenex Inc. (Torrance, CA, USA). ProSwift RP-1S organic polymer (polystyrene–divinylbenzene) based column (50×4.6 mm) was purchased from Thermo Scientific (Sunnyvale, CA, USA). New wide-pore silica-based monolithic research samples (C18, 100×4.6 mm, KN2229, VNr. 4463.06 and 4463.08) were generous gift from Merck KGaA (Darmstadt, Germany). Selected physico-chemical properties of these stationary phases are listed in Table 1. The columns are referred to in the paper as sub-2 μm fully porous, core-shell, organic monolith, and silica-based monolith columns.

Equipment, software

All measurements were performed using a Waters Acquity UPLC™ system equipped with a binary solvent delivery pump, an autosampler, and fluorescence detector (FL). The Waters Acquity system includes a 5-μL sample loop and a 2-μL FL flow-cell. The loop is directly connected to the injection switching valve (no needle seat capillary). The upper limit of flow rate with this system is 2 mL/min. The overall extra-column volume (V_{ext}) is about 15 μL as measured from the injection seat of the auto-sampler to the detector cell. The measured dwell volume is around 100 μL. The extra-column peak variance of this system in gradient elution mode was found to be negligible. Data acquisition and instrument control were performed by Empower Pro 2 Software (Waters).

Calculation and data transferring were achieved using Excel and OriginPro 8 templates.

Apparatus and methodology

Mobile phase composition and sample preparation

For the gradient separation of mAbs and their fragments, the mobile phase "A" consisted of 0.1 % TFA in water while the mobile phase "B" was 0.1 % TFA in acetonitrile.

Intact mAbs were injected without dilution, directly from the concentrated commercial solutions (10 mg/mL rituximab, 25 mg/mL bevacizumab, and 20 mg/mL panitumumab).

IgG monoclonal antibodies possess intramolecular disulfide bonds which were reduced with DTT. For this purpose, 0.05 mg of DTT was added to 100 μL mAb concentrated solution followed by an incubation at 30 °C for 60 min. Proteins were completely converted to the light-chain (LC) and heavy-chain (HC) components of the antibodies, ~25- and ~50-kDa fragments, respectively.

To prepare 25-kDa fragments, the reduced antibody (HC and LC) was digested by the addition of papain (diluted to 100 μg/mL with water) to give a final protein/enzyme ratio of ~100:1 (m/m%), the final digestion volume was 200 μL and was directly injected using low-volume insert vials. The digestion was carried out at 40 °C for 5 h. This digestion process yields three main fragments of ~25 kDa, namely the native LC, the single-chain Fc (sFc), and the Fab portion of the HC (Fd). This sample (containing the three 25-kDa fragments) was used for peak capacity evaluation. This approach (generating of ~25 kDa domains) is generally known as the combinatory strategy (combination of intact mAb reduction and papain digestion) and could be used for the characterization and comparison of mAbs by RPLC.

Deamidated mAb samples were created by adding 5 μL 0.1 M HCl into 95 μL rituximab concentrated solution. The samples were stored under ambient conditions for 24 h; then

Table 1 Physical–chemical properties of the compared columns

	Wide-pore silica-based monolithic research samples	Proswift RP-1S (PS-DVB monolith)	BEH300 1.7 μm C18 (packed, fully porous)	Aeris WP 3.6 μm C18 (packed, core-shell type)
Column dimension	100×4.6 mm	50×4.6 mm	150×2.1 mm	150×2.1 mm
Surface chemistry	C18	Phenyl	C18	C18
Particle size/macro-pore size (μm) measured	1.2	1.0	1.9[a]	3.6 [a]
Average pore size/mesopore size (Å)	~257	n.a.	~290	~200
Total pore volume (cm^3/g)	2.93[b]	n.a.	0.69 [b]	0.08
Total porosity	0.85	0.54	0.67	0.51
Max temperature (°C)	60	70	80	90
pH range	1.5–7.6	1–14	1–12	1.5–9
Max pressure (bar)	200	200	1000	600

[a] Measured by the authors [53]

[b] Measured and provided by the vendors

the antibody was reduced to LC and HC fragments by adding 0.05 mg DTT followed by incubation at 30 °C for 60 min.

Heat-stressed degraded samples were produced by incubating the reduced and digested sample at 95 °C for 60 min. The final sample contains several degradation products of the 25-kDa fragments.

Recovery study, the effect of temperature

On column adsorption of intact mAbs and their HC and LC fragments was evaluated in a systematic way. The adsorption on core-shell and sub-2 μm porous materials was presented in a previous study [30]. In this current paper, we compared the adsorption properties of the organic and silica based monolithic columns. A difficulty could occur when comparing the recovery of these monolithic and packed columns, due to the differences in their internal column diameter, column volume, and porosity. The monolithic columns have 4.6 mm ID while the others are packed in 2.1 mm ID columns. Keeping the same linear velocity on these columns means a difference in flow rate, in agreement with the basic rules of geometrical method transfer [31]. On the other hand, the injected volume also has to be adjusted in agreement with column dimensions.

When comparing the recovery on the different columns, the most evident measure is the observed signal intensity (e.g., peak area) of the given compound. But in the case of UV or FL detection, the observed peak area is a function of mobile phase flow rate and also depends on the injected quantity. Therefore, the direct comparison of recoveries between columns having different dimensions is hardly feasible. Hence, we compared the recovery only on the two monolithic columns; 1 and 0.5 μL were injected on the 10- and 5-cm-long columns, respectively (considering their column volume). Since their diameters are identical, the same flow rate (1.4 mL/min) was applied for practical purposes (please note, that in this case the linear velocity was not identical on the two columns since their porosity is highly different).

Keeping the quality of a gradient separation on columns having different lengths, diameters, and porosity (phase ratio), the rules of linear solvent strength (LSS) theory and general geometrical method transfer have to be applied [31, 32].

Short gradient runs (5 min on the 5-cm-long organic- and 10 min on the 10-cm-long silica based monoliths) were carried out at different temperatures ranging from 40 °C up to the upper temperature limit of the columns (in 10 °C steps). According to the providers, the silica-based prototype material is stable up to 60 °C, while the organic monolith is stable up to 70 °C. Samples (1 and 0.5 μL) were injected, and FL detection (excitation at 280 nm, emission at 360 nm, 20 Hz) was performed. Generic linear gradient from 30 % to 40 % B was applied. The obtained peak areas (normalized to the maximum observed area as 100 %) were plotted as a function of temperature.

Column efficiency, peak capacity, and separation impedance

The column efficiency in gradient elution mode is generally described by the peak capacity. Peak capacity was first described by Giddings [33] and soon put to good use by Horvath for gradient separations [34]. For the comparison of column efficiency in gradient elution mode, several theoretical and experimental expressions can be found in the literature [35–40].

Peak capacity depends on various experimental parameters. Among them, the gradient steepness, flow rate, and temperature play crucial role. For large biomolecules (such as antibodies and their fragments), temperature should be set as high as possible for both recovery and efficiency issues but is limited by either the instrument or the column thermal stability. Therefore, the optimization of gradient protein separation generally means the investigation of the effect of flow rate and gradient steepness on the efficiency (peak capacity). It seems that, for large biomolecules, the effect of gradient steepness on the separation power is more dominant than the effect of flow rate. If the very low diffusivity of large molecules (diffusion in the bulk mobile phase D_M and diffusion in the pores D_S or effective diffusion D_{eff}) is considered, it is easy to demonstrate that the lower the flow rate (or linear velocity), the higher the obtainable peak capacity is, in analogy with isocratic plate height (H) equations [19, 34]. Large molecules do not show an optimum (minimum) in isocratic H-u representations [19, 41, 42].

In order to have comparable results with these columns of different dimensions at different flow rates, the rules of LSS theory and geometrical method transfer were applied [31, 32].

The next formula was used to calculate the gradient steepness (s) for the given conditions:

$$s = (\phi_e - \phi_0) \cdot \left(\frac{L}{t_g - t_0}\right) \cdot u = \beta \cdot L \cdot u \qquad (1)$$

where Φ_0 is the initial mobile phase composition and Φ_e is the final mobile phase composition, L is the column length, t_g is gradient time, t_0 is column dead time, u is linear velocity and β is the so-called time steepness of the linear gradient.

For the peak capacity measurements, the solvent strength was varied linearly with gradient times. The peak capacity of each column was investigated at two different linear velocities ($u_1 \sim 5.8$ cm/min and $u_2 \sim 11.6$ cm/min; these values correspond to flow rates that are generally used in practical separations, approximately $F_1 \sim 0.2$ mL/min and $F_2 \sim 0.4$ mL/min for the narrow bore 2.1 mm ID columns and $F_1 \sim 1$ mL/min and $F_2 \sim 2$ mL/min for the standard bore 4.6 mm ID columns). The gradient steepness at u_1 was set

between $s \sim 10$ and $s \sim 112$ %B*cm^2/min^2 in 7 different experimental points, while at u_2, it was set in the range of $s \sim$ 39–460 %B*cm^2/min^2 again at seven different values. Beside the flow rate and gradient steepness, the effect of temperature on column efficiency was also evaluated since it is a key parameter in protein separation. In the first comparison, all columns were thermostated at 60 °C (this is the limitation of the new wide-pore silica-based monolithic research sample) and compared at the same temperature. Since the diffusivity (and therefore the separation efficiency) of large analytes strongly depend on the temperature, it is of great interest to compare the performance of these columns at their maximum temperature. In this comparison, the temperature was set at 60 °C for the silica-based monolithic column, 70 °C for the organic monolith, 80 °C for the sub-2 μm porous, and 90 °C for the core-shell columns. The injected volume was set in agreement with the rule of geometrical transfer. It was equal to 1 μL for the silica-based monolithic column, 0.5 μL for the organic monolith, and 0.3 μL for the two packed columns.

The above explained conditions can be used to directly compare the efficiency of these columns of different dimensions in gradient elution mode, for protein separation. However, the experimentally observed peak capacity (n_C) values are not comparable since peak capacity also depends on column length. Therefore, the peak capacities extrapolated to 1 m column length ($n_{C,M}$) were considered in this comparison. When maintaining constant the gradient steepness, the following formula can be written:

$$n_{c,M} = n_c \sqrt{\frac{100}{L}} \tag{2}$$

Where $n_{c,M}$ is the peak capacity extrapolated to 1 m length and L is the column length in centimeters.

Peak capacities were experimentally determined from the gradient time and the average peak widths measured at 50 % height ($w_{50\ \%}$). The following equation was used to estimate the peak capacity based on peak widths at 4σ, corresponding to a resolution of Rs=1 between consecutive peaks:

$$n_c = 1 + \frac{t_g}{1.699 \cdot w_{50\%}} \tag{3}$$

The sample containing the three main fragments of ~25 kDa, (LC, sFc, and Fd) of rituximab was injected in this comparative study. Therefore, the peak width of the three main peaks was used for calculating an average peak capacity. To avoid the imprecision associated with the measurement of peak widths at baseline for antibody fragments often containing closely related variants, the peak width at half height was preferred in this study. Thus, impurities present in the sample and partially resolved from the main component did not confuse the measurement of peak capacity values.

During the experiments, Φ_e–Φ_0 was kept constant (10 %) for all columns. But for maintaining similar apparent retention on the different stationary phases, Φ_0 was set at 28 %B on the silica-based monolithic column, 27 %B on the organic monolith column, and 29 % on the two packed columns.

When comparing the efficiency of these columns, the peak capacity *per* meter was plotted against the gradient span (expressed in time per column length dimension such as minute per meter). The gradient span (S_g) in this case was calculated as:

$$S_g = t_g \left(\frac{100}{L} \right) \tag{4}$$

The column performance also depends on column permeability (K_v) and retention time, the latter being related to column dead time and/or gradient time. Therefore, peak capacity plots do not give information about the overall quality of the separation (e.g., achievable separation time) but only about the reachable peak widths.

When the flow rate is changed but the gradient steepness is kept constant, the so-called gradient kinetic plots can be easily constructed. Different gradient kinetic plots have been presented by Wang et al., Zhang et al., Haddad et al., Ruta et al., and Desmet et al. [43–48]. In our case, it was more interesting to investigate the opposite case when experimental conditions corresponded to different gradient steepness at constant flow rate. By analogy to Knox's separation impedance concept [49], similar representation of kinetic performance can be constructed by calculating the peak capacity *per* unit time and *per* unit pressure values, according to the next formula [19, 50, 51]:

$$PPT = \frac{n_c}{t_g \cdot \Delta P} \tag{5}$$

where PPT is the peak capacity *per* unit time and *per* unit pressure value and ΔP is the column pressure drop (the maximum pressure measured during the gradient program, corrected for extra-column pressure drop). Plots of PPT as a function of gradient spans were constructed and compared for two sets of linear velocity and two sets of temperatures (similarly to peak capacity plots, the PPT values were extrapolated for 1 m column length (PPT_M) in order to normalize these values and make them independent on column length).

Evaluating the loading capacity of the columns

The loading capacity of the different materials (monolith, fully porous, and core-shell) was compared under real-life conditions. Reduced rituximab sample was used to evaluate the loadability of these columns. Different amounts of the antibody (2, 5, 10, 20, 40, 60, 80, 100, and 200 μg) were

injected. The experiments were conducted at one given linear velocity (u_1 ~ 5.8 cm/min) with a given gradient span (S_g = 100 min/meter). For the experiments, Φ_e–Φ_0 was kept constant (10 %). Similar apparent retention was maintained on the different stationary phases. All columns were thermostated at 60 °C. The chromatograms were recorded at 360 nm (20 Hz, excitation at 280 nm). Finally, the loadability was evaluated by measuring and plotting the peak widths and the percent change in peak capacity as a function of the loaded protein amount (nanograms). For a fair comparison, on the *x*-axis, the loaded amount *per* column volume (expressed in nanograms per cubic millimeter) was indicated.

Results and discussion

Recovery, adsorption of antibody fragments

In a previous study dealing with the analysis of mAbs in RPLC [30], we have demonstrated that the adsorption phenomenon with intact mAbs and their fragments could be problematic since it was significantly higher, compared with proteins of equivalent size. According to this study, the recovery was directly related to the size of intact or digested/reduced mAbs, the largest fragments being much more affected by adsorption. Another conclusion from this work was that the low recovery of mAbs in RPLC was predominantly attributed to strong secondary interactions (ionic and hydrogen bonds) with the stationary phase, while the effect of alkyl chain hydrophobicity (C18 versus C4) was less relevant. The best solution to decrease the importance of adsorption was to increase the mobile phase temperature in order to reduce the strength of secondary interactions [53].

Because the two monolithic columns have 4.6 mm while the packed columns have 2.1 mm ID, it is impossible to directly compare these four columns. For this reason, and also to avoid repeating some data previously published, we have only measured the adsorption on both the silica-based monolith and the organic monolith. The recoveries obtained with the column packed with 3.6 μm core-shell particles possessing a wide pore size distribution and that of fully porous 1.7 μm particles, with pore size of ~300 Å can be found elsewhere [30], and were obtained using the same experimental setup and similar model antibodies and their fragments.

Figure 1 shows the data obtained for two intact mAbs and their fragments, namely rituximab and bevacizumab. The recoveries were expressed as normalized peak areas and were investigated as a function of mobile phase temperature. The temperature ranges were 40–60 °C for the silica-based monolith and 40–70 °C for the organic monolith. In agreement with the previous study [30], recoveries were much more critical for intact mAb of 150 kDa followed by HC of 50 kDa and the LC of 25 kDa. For example, the recovery on intact rituximab at 60 °C was equal to less than 10 % on the silica-based monolith while the recovery values increased to 52 % and >99 % for HC and LC, respectively. Similar behavior was observed on the organic monolithic column but with better recovery in terms of absolute values. In addition, the curves were very similar for both rituximab and bevacizumab, but the adsorption seemed to be slightly more pronounced for bevacizumab.

On the other hand, the recoveries were significantly improved with elevated temperature, and adsorption was

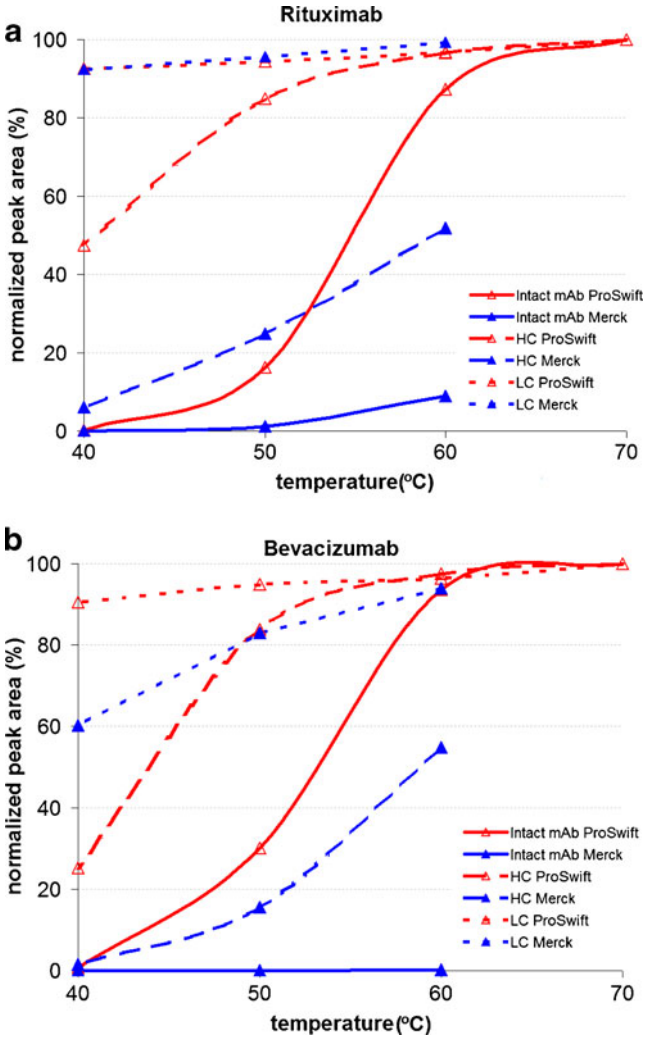

Fig. 1 Recovery of **a** rituximab and its heavy (HC) and light chains (LC) and **b** bevacizumab and its heavy (HC) and light chains (LC) (normalized peak areas against column temperature). Columns: organic monolith (ProSwift RP-1S) and wide-pore silica-based monolith (Merck), temperature: from 40 °C up to 70 °C, injected volume: 0.5 μL, detection: fluorescence (excitation at 280 nm, emission at 360 nm). Mobile phase A—0.1 % TFA in water, mobile phase B—0.1 % TFA in acetonitrile. Gradient: from 30 % to 40 % B in 5 min (for ProSwift RP-1S 5 cm column) and in 10 min (for 10 cm long Merck wide-pore monolith research sample), flow rate, 1.4 mL/min

generally acceptable in the temperature range between 60 and 70 °C, except for the intact mAbs on the silica-based monolith. As example, on the latter, the recovery of intact rituximab was increased from 0 % to 9 % when raising temperature from 40 to 60 °C, while the recovery of HC and LC was increased from 6 % to 51 % and from 92 % to 99 % between 40 and 60 °C, for the same stationary phase. A good solution to further limit recovery issues would be to have silica-based monolithic columns stable at higher temperatures.

Finally, as reported in Fig. 1, some significant differences in terms of adsorption/recovery were observed between the silica-based and the organic monolith. Indeed, at a temperature of 60 °C, the recoveries on intact rituximab were equal to 9 % and 87 % for the silica-based and the organic monolith, respectively. The same behavior was also observed on mAb fragments. This observation was probably related to the ion exchange capability of both columns and also probably to the hydrophobicity of the material (phenyl versus C18). Indeed, even if the silica-based monolith employed in the present study was endcapped, there should still be a significant number of residual silanols and thus, can participate in hydrogen-bonding interactions. According to the observations made on recovery, the amount of negatively charged groups is probably significantly higher at the surface of the silica-based compared with the organic monolith. Another explanation for the difference of recovery could be the difference in column chemistry and hydrophobicity. In fact, the silica-based monolith is bonded with C18 chain while the organic-based one possesses phenyl bonding, and additionally, there are no stagnant zones (mesopores) in the organic polymer monolith. There is an evident difference of hydrophobicity between such bonding that could also contribute to the better recoveries observed on the organic monolith.

Column efficiency in gradient mode for antibody fragments

In this section, a systematic study presents the peak capacity and gradient separation impedance (PPT) of silica-based wide-pore monolith, organic monolith, a wide-pore sub-2 μm fully porous material, and a 3.6 μm core-shell material. Table 1 summarizes physical–chemical properties of these columns.

This comparison allows us to directly compare the performance of these stationary phase materials possessing different structures and morphologies, in gradient elution mode. In practice, proteins are generally separated in gradient elution mode at elevated temperature. Elevated temperature is beneficial because it decreases the strength of secondary interactions between residual silanols and positively charged biomolecules. Moreover, the use of high temperature strongly enhances analyte diffusion. Furthermore, ion-pairing reagent, namely TFA, was added to the mobile phase to improve peak shape in the case of proteins separation. For the reason of emulating real-life conditions, a minimal column temperature of 60 °C was considered; 0.1 % TFA was added to the mobile phase, and gradient spans varied between S_g=50 and 600 min/m at u_1~5.78 cm/min and S_g=25 and 300 min/m at u_2~11.56 cm/min, which are fairly common in the current practice. (For better understanding, this S_g range corresponds to gradient times ranging between 7.5 and 90 min for a 150×2.1 mm column at 0.2 mL/min flow rate.) Beside the gradient steepness and flow rate, the effect of temperature was also evaluated. In a first instance, all the columns were thermostated at 60 °C (maximum recommended temperature for the silica-based monolith), and their efficiencies were compared. Then, the performance of the columns was measured at their maximum operational temperature. The test solution was a reduced and papain-digested rituximab that contains three main fragments of around ~25 kDa (LC, sFc, and Fd domains).

The influence of the gradient steepness and linear velocity on column performance was investigated under several gradient elution conditions. These experimental variables are directly related to the mobile phase flow-rate and the gradient time duration which are often used to adjust a proper separation in practical work. The former has a direct influence on the peak width while gradient duration plays an important role on the resolution as it affects the retention factor of the solute in the mobile phase composition upon elution. It should be stressed that these conditions are not meant to maximize the peak capacity for any particular column or compound, as sometimes higher peak capacity can be achieved by choosing longer gradient times or lower flow rates. Instead, we merely wanted to identify a set of conditions allowing a fair comparison within a practically acceptable time frame.

Figure 2a shows the obtained peak capacity *per* meter values as a function of gradient span at a relatively low linear velocity (u_1~5.8 cm/min) for all columns. The organic monolith gave the lowest peak capacity with a maximum peak capacity of $n_{c,M}$~360 reached with the S_g=600 min/m gradient span (that corresponds to a ~30 min long gradient for the 50×4.6 mm column). The silica-based wide-pore monolith showed slightly better performance. The sub-2 μm fully porous material performed very similar peak capacity ($n_{c,M}$~405 at S_g=600 min/m) than the silica-based monolith. Finally, significantly higher efficiency was attained with the core-shell material, and the highest peak capacity ($n_{c,M}$~490) was achieved.

When the mobile phase velocity was increased (u_2~11.6 cm/min), the two packed columns outperformed the two monolith columns in terms of peak capacity (Fig. 2b). At this linear velocity, the same efficiency was obtained for both monolith columns within the whole investigated gradient span range. At the applied maximum gradient span,

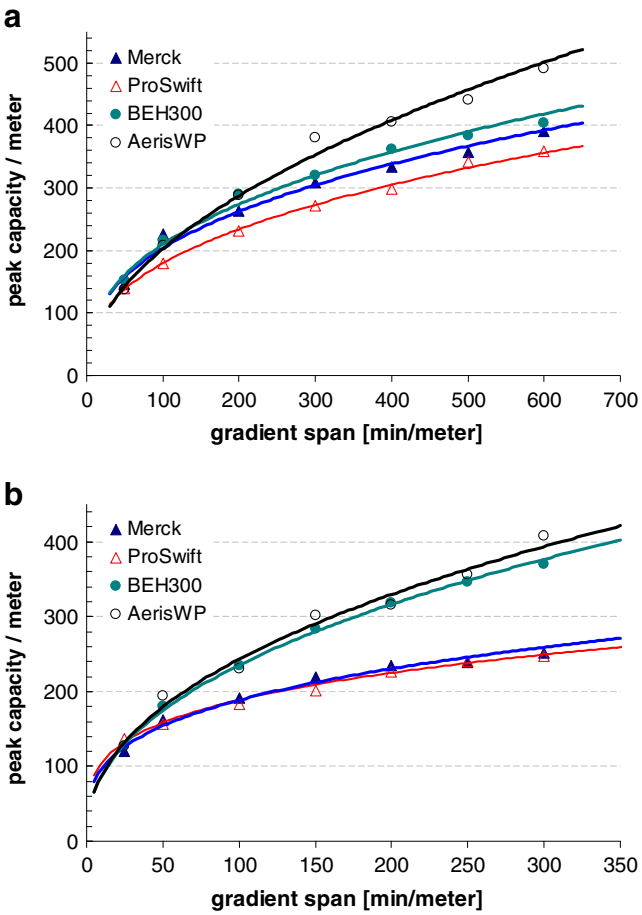

Fig. 2 Peak capacity plots of rituximab fragment sample at u_1~5.8 cm/min (**a**) and at u_2~11.6 cm/min (**b**) linear velocity. Columns: wide-pore silica-based monolith (Merck), ProSwift RP-1S, BEH300 C18, and Aeris WP; temperature, 60 °C for all columns. Other experimental conditions are specified in section on "Column efficiency, peak capacity, separation impedance"

the packed columns outperformed the monolith columns by a factor of 1.6. There was a remarkable loss in peak capacity at this higher linear velocity compared with the values obtained at low velocity (Fig. 2b and a). In the case of the silica-based monolith column, the loss was about 40 %, while this decrease was 23 % with the organic monolith column and around 20 % with the core-shell material while it was nearly negligible (7–8 %) with the fully porous sub-2 μm column. The significant efficiency loss of the core-shell material compared with the packed fully porous sub-2 μm one can probably be explained with its relatively large particle size (d_p=3.6 μm), since the contribution of the mass transfer resistance to the total H is a function of particle diameter.

Another representation of column efficiency is shown in Fig. 3. In this case, the quality of separation is considered on the basis of peak capacity, column permeability, and analysis time as well. Figure 3a shows the peak capacity *per* pressure and time unit (PPT) values as a function of the gradient span at u_1~5.8 cm/min, and at 60 °C for all columns. In this representation, the higher the PPT value, the lower the "separation impedance" is. These plots illustrate that the fastest separation can be achieved with the core-shell and the new silica-based monolith columns. These two columns drastically outperformed the sub-2 μm fully porous and the organic monolith columns. Surprisingly, the organic monolith showed two times lower permeability than the silica-based monolith, in spite of the slight difference in their average macropore size (~1 μm for the organic and 1.2 μm for the silica-based monolith). The sub-2 μm porous material showed a relatively poor efficiency due to its very low permeability compared with the other materials.

When increasing the mobile phase velocity (Fig. 3b), the 3.6 μm core-shell material provided the best efficiency and therefore offered the chance of the fastest separation. The silica-based monolith also provided good performance,

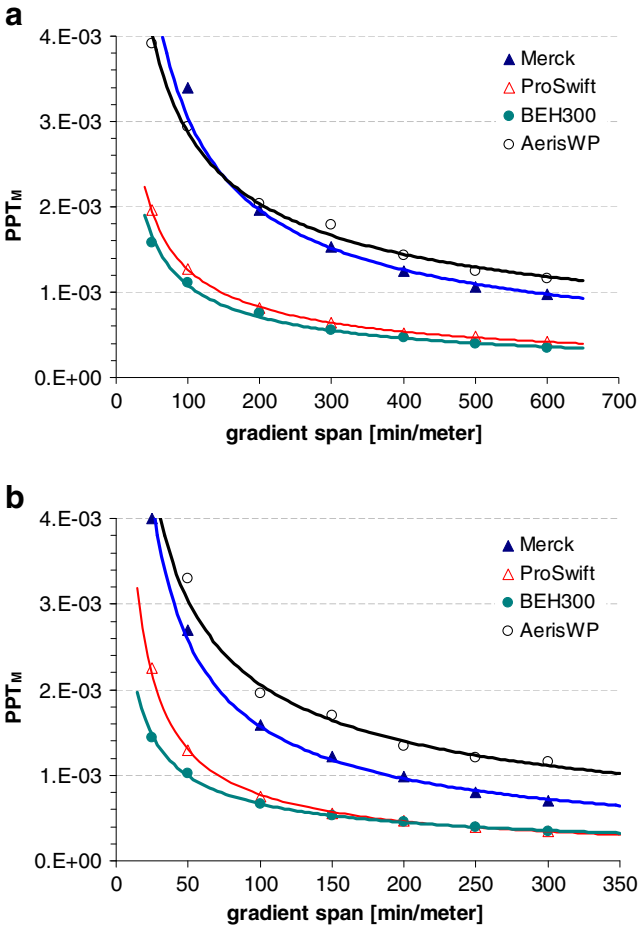

Fig. 3 Gradient separation impedance (peak capacity per time unit and per pressure unit versus gradient steepness) plots of rituximab fragment sample at u_1~5.8 cm/min (**a**) and at u_2~11.6 cm/min (**b**) linear velocity. Columns: wide-pore silica-based monolith (Merck), ProSwift RP-1S, BEH300 C18, and Aeris WP; temperature, 60 °C for all columns. Other experimental conditions are specified in section "Column efficiency, peak capacity, separation impedance"

while the fully porous sub-2 μm and the organic monolith gave the lowest *PPT* values (the highest separation impedance). When comparing these two latter columns, they present the same separation impedance when high peak capacity is required for a given separation (corresponds to the range when $S_g \geq 200$ min/meter) while the organic monolith significantly outperforms the sub-2 μm porous material when fast gradients are applied (e.g., $S_g < 100$ min/m).

When working at the maximal temperature of the different stationary phases, the efficiency of protein separations can be considerably improved. Figure 4 presents the peak capacity *per* meter values obtained at their maximum operational temperature. Applying low flow rate (Fig. 4a), the maximum peak capacity of $n_{c,M} \sim 725$ was reached with the sub-2 μm porous column (T=80 °C) at $S_g = 600$ min/m gradient span. The core-shell column (T=90 °C) reached its limitation in terms of peak capacity at $S_g \sim 500$ min/m gradient span. The maximum peak capacity that can be achieved with this core-shell material is $n_{c,M} \sim 700$. However, it has to be mentioned that, in $S_g = 50$–500 range, the core-shell material outperformed the sub-2 μm fully porous packing. The silica-based monolith (T=60 °C) and the organic monolith (T=70 °C) provided the same peak capacity. With the monoliths, $n_{c,M} \sim 400$ was reached when applying the longest gradient run.

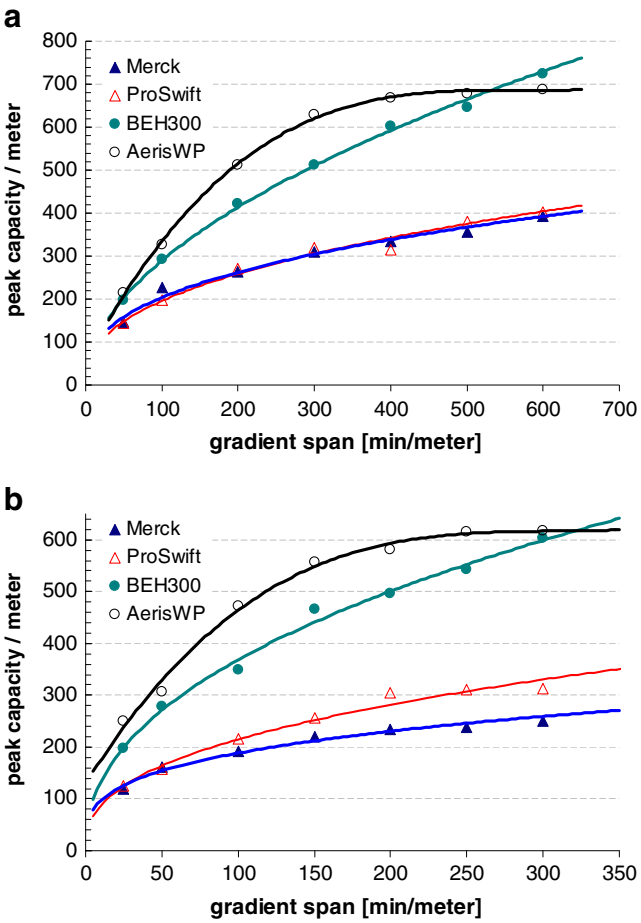

Fig. 4 Peak capacity plots of rituximab fragment sample at $u_1 \sim 5.8$ cm/min (**a**) and at $u_2 \sim 11.6$ cm/min (**b**) linear velocity. Columns and temperature: wide-pore silica-based monolith (Merck) (60 °C), ProSwift RP-1S (70 °C), BEH300 C18 (80 °C), and Aeris WP (90 °C). Other experimental conditions are specified in section "Column efficiency, peak capacity, separation impedance"

It is important to mention that temperature has indeed a strong impact on efficiency of gradient RPLC protein separations. The maximum achievable peak capacity with the core-shell material was improved by a factor of 1.4 at T=90 °C compared with T=60 °C. With the sub-2 μm fully porous material, the gain in column efficiency was more pronounced. The maximum peak capacity was increased by a factor of 1.8 between T=80 and 60 °C. In the case of organic monolith column, 1.12 times higher peak capacity was attained when working at T=70 °C compared with T=60 °C.

Figure 4b shows the peak capacity of the four columns at their maximum temperatures and at elevated mobile phase velocity. Again, at higher mobile phase velocity, the efficiency became markedly lower compared with low mobile phase velocity. The packed columns showed very similar behavior that was shown and explained at Fig. 4a. However, the difference between the two monolith columns was more pronounced. At a mobile phase velocity of $u_2 \sim 11.6$ cm/min, the organic monolith gave 90 % of the peak capacity that was achieved at $u_1 \sim 5.8$ cm/min, while the silica-based monolith performed only 65 % of that attained at half the mobile phase velocity. Therefore, when applying high mobile phase velocity, the organic monolith outperformed the silica-based monolith in terms of achievable peak capacity.

Working at the maximum temperature and comparing the column performance in PPT plots (Fig. 5), the benefit of core-shell material became obvious. This 3.6 μm superficially porous material provided high peak capacity, and beside this fact, its permeability is also favorable because of its relatively large particles. The other important feature of this material is its high temperature stability that enables to perform very efficient and fast antibody separations. At low mobile phase velocity (Fig. 5a), the new silica-based monolith showed some benefits against the organic monolith and sub-2 μm porous materials, but this gain was less important when working at a higher flow rate (Fig. 5b). In this case, the silica-based monolith, the organic monolith, and the sub-2 μm fully porous packed column presented very similar impedance and produced lower performance than the core-shell type 3.6 μm packing.

Evaluation of the loading capacity

Sample loading capacity is proportional to the stationary phase volume or phase ratio, and it is expected that the

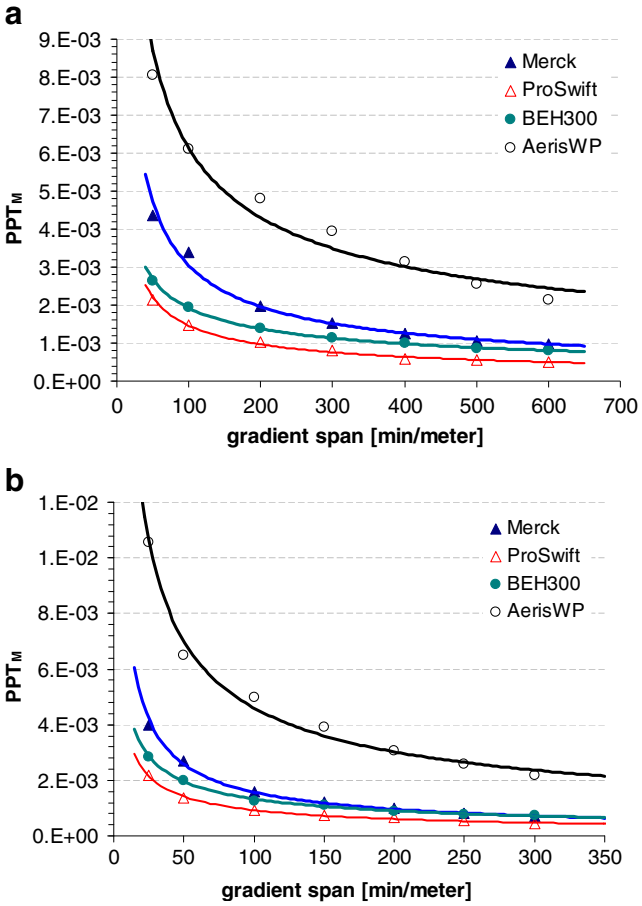

Fig. 5 Gradient separation impedance (peak capacity per time unit and per pressure unit versus gradient steepness) plots of rituximab fragment sample at $u_1 \sim 5.8$ cm/min (**a**) and at $u_2 \sim 11.6$ cm/min (**b**) linear velocity. Columns and temperature: wide-pore silica-based monolith (Merck) (60 °C), ProSwift RP-1S (70 °C), BEH300 C18 (80 °C), and Aeris WP (90 °C). Other experimental conditions are specified in section "Column efficiency, peak capacity, separation impedance"

phase ratio of monolithic and packed columns could be very different. Moreover, the porosity of silica-based (ε=0.85) and organic polymer-based monoliths (ε=0.54) were also very different. In the case of fully porous and core-shell type packed columns, the volume of the porous parts of the stationary phase is also completely different. The volume fraction of the porous material of the shell in the column is $1-(R_i/R_e)^3$, where R_e and R_i are the radii of the solid core and the particle, respectively. The volume fraction of the porous shell in the case of Aeris WP particles was estimated at about 34 %.

Overloading of the stationary phase is always more significant with ionized compounds in RPLC separations [52]. Proteins can be retained on both ionic and hydrophobic sites of the stationary phase, therefore the lower expected loadability of the core-shell type material and silica-based monolith can probably be compensated by their apparently higher ion exchange capability, compared with the fully porous hybrid sub-2 μm (BEH) and organic polymer-based (ProSwift) materials [53]. An additional consideration is that differences in pore size distribution of the sorbents can also play a significant role in overloading, since exclusion of proteins from pores can induce serious overloading effects.

Hence, because of the huge differences in stationary phase structure/morphology of the compared materials, the evaluation of the sample loading capacity is of interest but could be difficult to explain. The loading capacities of the different materials were compared in a systematic way. The experimental conditions were described in the section "Evaluating the loading capacity of the columns."

Figure 6a shows the absolute change in peak width of the light-chain fragment of rituximab against loaded amount. In this comparison (under the given conditions), the silica-based monolith provided somewhat broader peaks ($w_{1/2} \sim$ 0.13 min) than the other three columns ($w_{1/2} \sim 0.10$ min). In the case where the loaded amount of this light-chain fragment was more than 10 ng/mm^3, the peak width on the organic monolith column started to broaden more rapidly

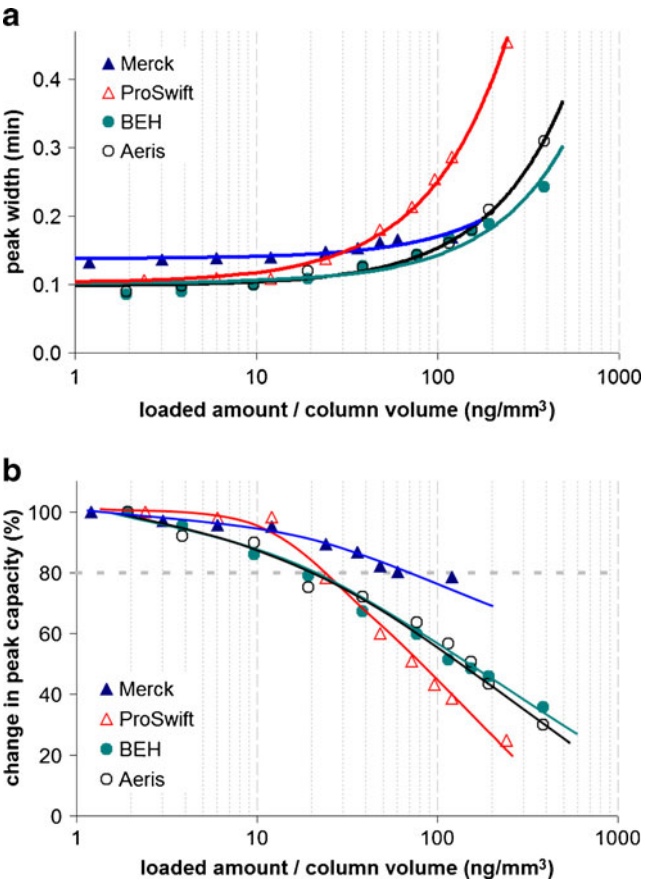

Fig. 6 Absolute of the peak width of light-chain fragment (**a**) and relative change in peak capacity (**b**) in function of the loaded mass/column volume. Columns: wide-pore silica-based monolith (Merck), ProSwift RP-1S, BEH300 C18, and Aeris WP; temperature, 60 °C for all columns. Other experimental conditions are specified in section "Evaluating the loading capacity of the columns"

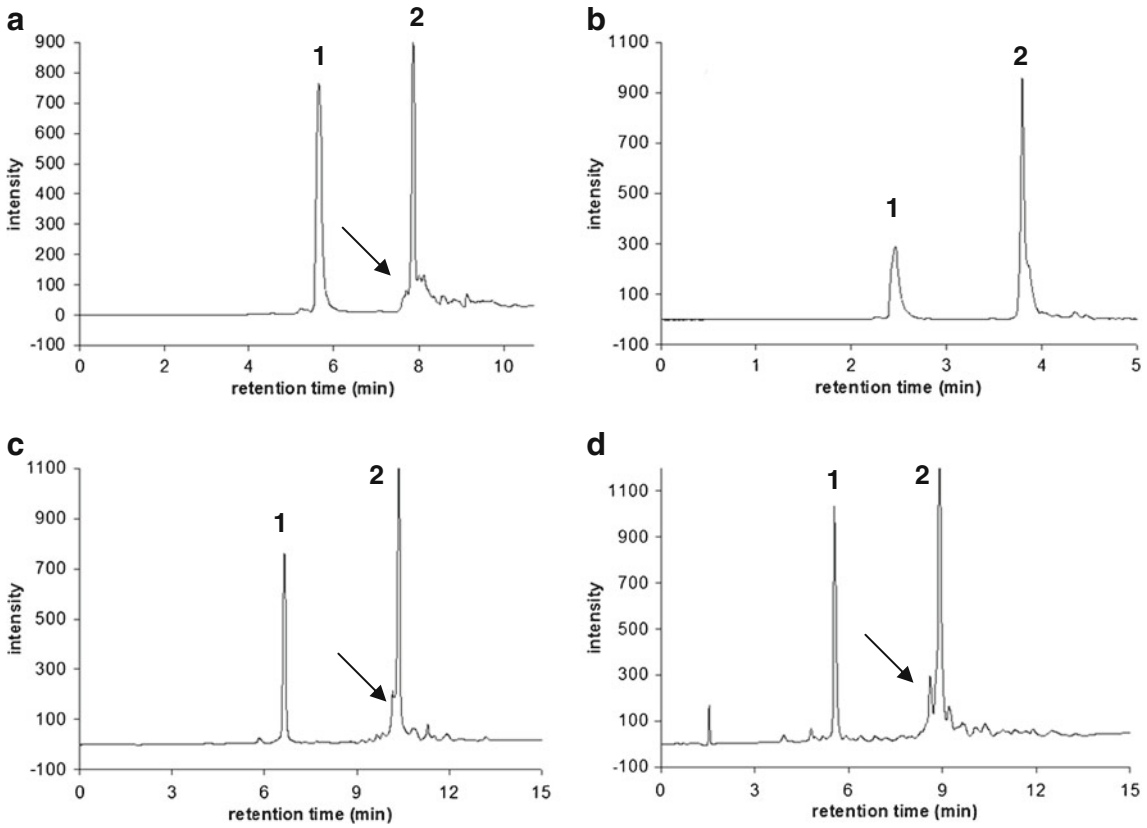

Fig. 7 Separation of LC (peak *1*) and HC (peak *2*) fragments and some variants of deamidated rituximab sample. The supposed deamidated form of the LC is indicated with *arrows*. On the 5-cm-long ProSwift column (**b**), no change was observed in the chromatographic profile when injecting the deamidated and non-deamidated samples. Columns and applied temperature: wide-pore silica-based monolith (**a**) at 60 °C, ProSwift RP-1S (**b**) at 70 °C, BEH300 C18 (**c**) at 80 °C, and Aeris WP (**d**) at 90 °C; linear velocity, $u \sim 5.78$ cm/min; detection: fluorescence (excitation at 280 nm, emission at 360 nm). Other experimental conditions are specified in section "Applications, examples"

compared with the other columns. When the loaded amount was larger than 30 ng/mm^3, the silica-based monolith gave sharper peak than the organic monolith. Surprisingly, the change in absolute peak width was less pronounced on the silica-based monolith than on the packed columns. When the loaded amount was comprised between 100 and 200 ng/mm^3, the silica monolith performed same peak width as the packed columns.

Figure 6b shows another representation of loading capacity, namely the relative change in peak capacity as a function of loaded amount. This figure obviously confirms that overloading is more critical in the case of organic monolith while the silica monolith is less problematic in terms of overloading. Unexpectedly, the fully porous and core-shell type materials showed the same behavior, in spite of the huge difference in their porous volume. Probably, the loadability on the core-shell material can be compensated by its relatively high ion-exchange activity and/or different pore size distribution. Since there is no criterion on setting the limits of column overloading, an arbitrary value of 20 % relative decrease in peak capacity was considered as acceptable. The core-shell, the sub-2 μm fully porous, and the organic monolith columns reached 20 % decrease in peak capacity when approximately 20–25 ng/mm^3 of the light-chain fragment was loaded and about 65–70 ng/mm^3 on the silica-based monolith.

As a conclusion, for ~25-kDa antibody fragment, the loadability of the columns can be ranked as: (1) new wide-pore silica-based monolithic, (2) the fully porous and superficially porous packed columns (BEH and Aeris WP), and (3) the organic monolith. This latter one showed approximately a threefold lower sample loading capacity than the new silica-based monolith. Probably, other type of proteins could show different behavior and the loading capacity of the columns ranked in a different way. In this study, we focused only on antibody fragments.

Applications, examples

Proteolytic digestion of a mAb (peptide mapping) followed by gradient RPLC-tandem mass spectrometry analysis ("bottom-up approach") is generally the method of choice for the identification and quantification of chemical modifications of mAbs [54, 55]. However, this approach is time-

consuming and can induce putative modifications during the complex and lengthy sample preparation [55]. Alternatively, the analysis of intact or fragmented mAbs requires very little sample preparation and can provide a high-throughput alternative to peptide mapping.

Using RPLC under reducing conditions, the LC generally elutes in a single sharp peak, while HC fragments elute often in heterogeneous peaks. Another current approach is the so-called limited proteolysis that means the analysis of IgG1 and IgG2 Fab and Fc domains using RPLC or RPLC–time-of-flight–mass spectrometry. This approach facilitates the confirmation of chemical and post-translational modifications such as N-terminal cyclization, oxidation, deamidation, and C-terminal processed lysine residues [20, 56–59].

A new combinatory strategy was presented by Yan et al. to analyze the heterogeneity of LC, sFc, and Fd of an IgG molecule released by papain cleavage under mild reducing conditions [60].

In this section, the performance of the four columns was investigated for a real monoclonal antibody separation. In the first example, rituximab was slightly deamidated and then reduced (see section on "Mobile phase composition and sample preparation"). The obtained chromatograms of the resulting LC and HC fragments are presented in Fig. 7 (experimental conditions are specified in section on "Applications, examples"). Please note that column lengths were different. Surely, a 10–15-cm-long organic monolith column would perform significantly better that the 5 cm one. The probable deamidated form of the HC (indicated with arrow in Fig. 7) can be slightly separated with the 1-cm-long silica-based monolith and with the 15-cm-long sub-2 μm fully porous columns and can be well resolved by using the 15-cm-long core-shell type column, using generic conditions.

The second example presents a comparison of the chromatographic profile of a heat-stressed, papain-digested, and reduced rituximab sample (see section on "Mobile phase composition and sample preparation"). This sample contains several variants/degradants of the LC, sFc, and Fd domains (Fig. 8). The two packed columns were able to resolve many of these fragments while the two monolithic columns can separate only a limited number of these degradants. In this example, the packed columns showed better performance than the monolithic columns (but there are significant differences in column lengths). Because of the favorable permeability of the new silica-based monolith column, coupling various columns in series could be a promising approach and probably could yield far better separation power.

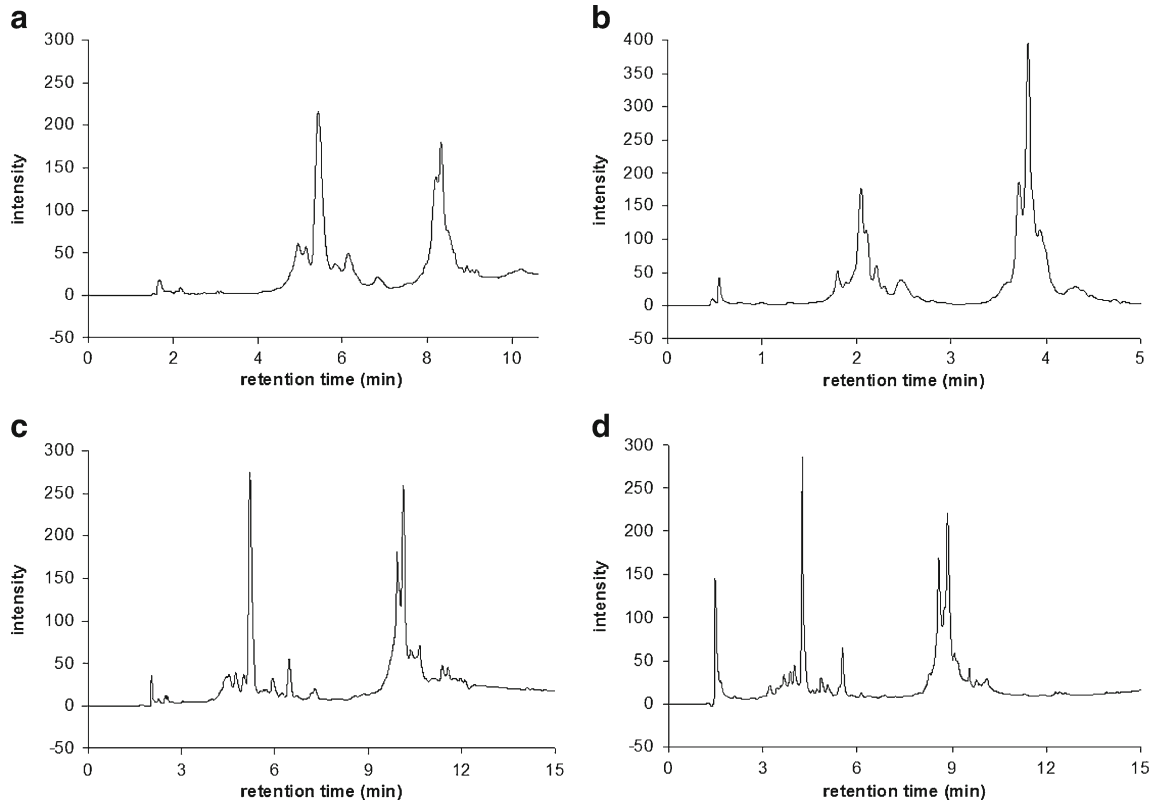

Fig. 8 Separation of several fragments and variants of heat-stressed-reduced and papain-digested rituximab sample. Columns and applied temperature: wide-pore silica-based monolith (**a**) at 60 °C, ProSwift RP-1S (**b**) at 70 °C, BEH300 C18 (**c**) at 80 °C, and Aeris WP (**d**) at 90 °C; linear velocity; $u \sim 5.8$ cm/min, detection: fluorescence (excitation at 280 nm, emission at 360 nm). Other experimental conditions are specified in section "Applications, examples"

Conclusion

Recent RPLC phases possessing significant differences in structure/morphology were evaluated for the analysis of intact mAbs (~150 kDa) and their fragments (~25–50 kDa). Two monolithic materials were considered, namely a prototype wide-pore silica-based column and a PS-DVB organic monolithic stationary phase. Two packed columns were also employed, namely a column packed with wide-pore fully porous particles of 1.7 μm and with wide-pore core-shell particles of 3.6 μm. Various model IgG1 and IgG2 mAbs were considered (rituximab, panitumumab, and bevacizumab), and the stationary phases were compared in terms of adsorption/recovery, kinetic performance in the gradient elution mode, and loading capacity.

In terms of adsorption/recovery, the packed columns were investigated in a previous study [30], and it was concluded that the adsorption was more critical on the silica-based core-shell material than on the hybrid sub-2 μm porous material probably because of a higher ion exchange capability on the former one. Regarding monoliths, the recoveries on organic monolith were excellent, above all when working at elevated temperature. On the other hand, some significant adsorption problems were observed with the prototype silica monolith, particularly with intact mAbs and large fragments (50 kDa).

Kinetic performance was compared using peak capacity measurements on various mAb fragments of ~25 kDa. Because the tested columns possessed different column lengths and internal diameters, some adaptations were made to the traditional gradient kinetic plot methodology. The performance was evaluated at low and high mobile phase linear velocity and

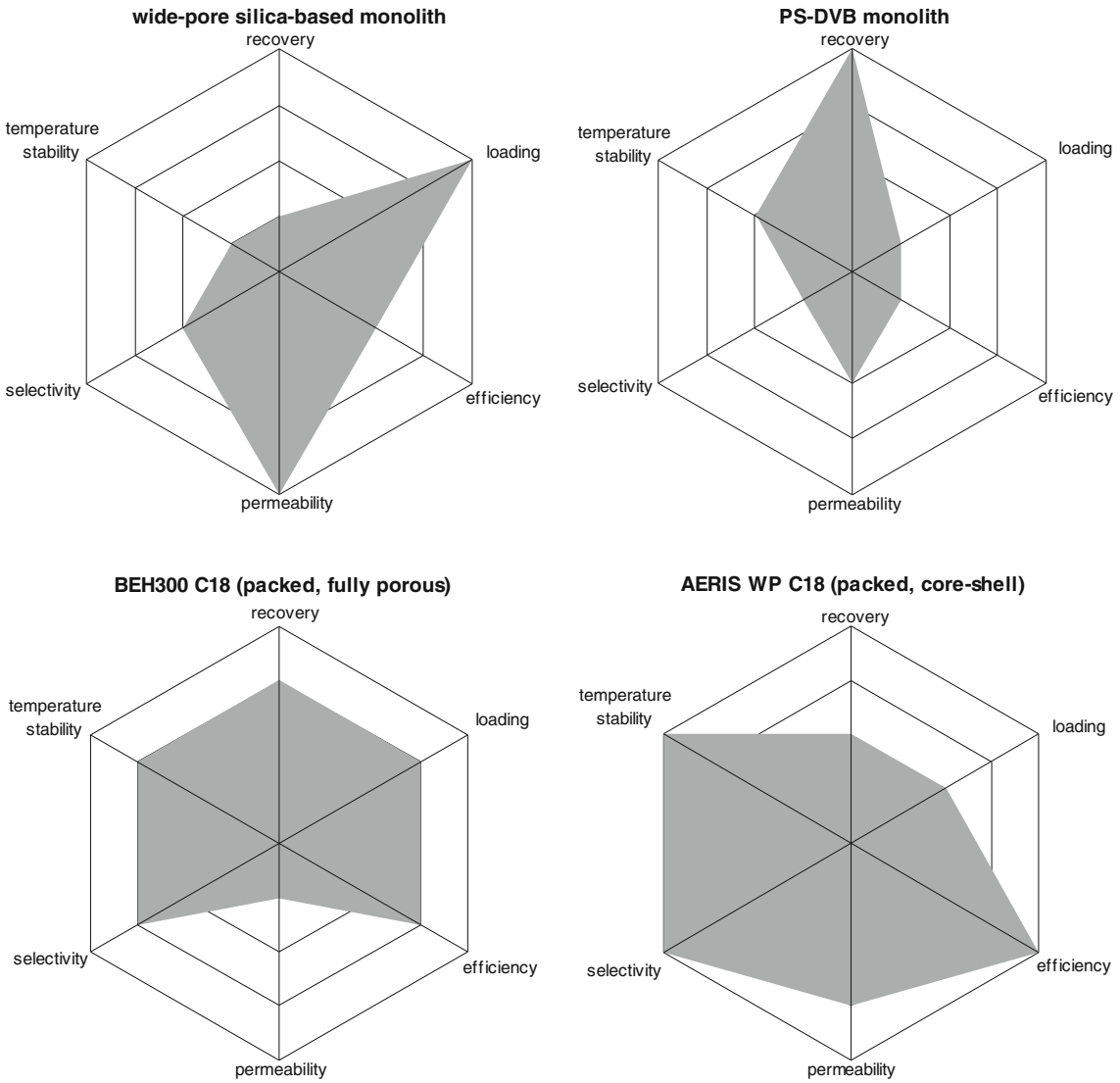

Fig. 9 Schematic comparison of the different column performance based on different parameters: recovery, loading capacity, efficiency, permeability, selectivity, and column temperature stability

using two mobile-phase temperatures, namely 60 °C for all columns or the maximal working temperature of all columns. Whatever the flow rate and mobile phase temperature were, the core-shell-type material outperformed the three other stationary phases. It provided high peak capacity and high permeability and was compatible with temperature up to 90 °C. On the other hand, the organic monolith suffered from a low permeability compared with the prototype silica-based monolith. Lastly, the sub-2 μm porous phase provided peak capacity close to that of 3.6 μm core-shell but was only able to work up to 80 °C, and its permeability was significantly lower.

Finally, the loading capacity also varied strongly between columns. In the case of mAb fragments, the prototype silica-based monolith was the most interesting one while the organic monolith overloaded more rapidly (threefold lower sample loading capacity than the prototype silica monolith). Despite very different particle morphologies, the loading capacity of packed columns was comparable.

Numerous parameters should be considered to adequately select the best column for a given purpose, including the recovery (adsorption), loading capacity, peak capacity (efficiency), permeability, selectivity, and thermal stability. To select the best column for a given application, all of these figures of merits have been combined in the spidergrams of Fig. 9 for the four investigated columns. To conclude, the four RPLC phases present some advantages and limitations, but all of them could be employed for the analysis of IgG1 and IgG2 mAb fragments (HC, LC, sFc, and Fd domains). This confirms the interest of RPLC approach for analyzing such large biomolecules.

Acknowledgments The authors wish to thank Dr. Karin Cabrera (Merck KGaA) for providing the new wide-pore silica-based monolithic research samples (C18, 100×4.6 mm, KN2229, VNr. 4463.06).

References

1. Guiochon G (2007) J Chromatog A 1168:101–168
2. Cabrera K (2004) J Sep Sci 27:843–852
3. Hjerten S, Liao JL, Zhang R (1989) J Chromatogr 473:273–275
4. Svec F, Frechet JMJ (1992) Anal Chem 64:820–822
5. Minakuchi H, Nakanishi K, Soga N, Ishizuka N, Tanaka N (1996) Anal Chem 68:3498–3501
6. Eeltink S, Wouters B, Desmet G, Ursem M, Blinco D, Kemp GD, Treumann A (2011) J Chromatog A 1218:5504–5511
7. Detobel F, Broeckhoven K, Wellens J, Wouters B, Swart R, Ursem M, Desmet G, Eeltink S (2010) J Chromatog A 1217:3085–3090
8. Hormann K, Müllner T, Bruns S, Höltzel A, Tallarek U (2012) J Chromatog A 1222:46–58
9. Knox JH (1977) J Chromatogr Sci 15:352–364
10. Poppe H (1997) J Chromatogr A 778:3–21
11. Giddings JC (1965) Anal Chem 37:60–63
12. MacNair JE, Lewis KC, Jorgenson JW (1997) Anal Chem 69:983–989
13. Jerkovich AD, Mellors JS, Jorgenson JW (2003) LC-GC Europe 16:20–23
14. Mazzeo JR, Neue UD, Kele M, Plumb RS (2005) Anal Chem 77:460–467
15. Guillarme D, Nguyen DTT, Rudaz S, Veuthey JL (2006) J Sep Sci 29:1836–1848
16. Eugster PJ, Guillarme D, Rudaz S, Veuthey JL, Carrupt PA, Wolfender JL (2011) AOAC Int 94:51–70
17. Novakova L, Vlckova H (2009) Anal Chim Acta 656:8–35
18. Staub A, Guillarme D, Schappler J, Veuthey JL, Rudaz S (2011) J Pharm Biomed Anal 55:810–822
19. Fekete S, Berky R, Fekete J, Veuthey JL, Guillarme D (2012) J Chromatogr A 1236:177–188
20. Krull IS, Rathore A (2011) LCGC North Am 29:838–852
21. Fekete S, Fekete J, Ganzler K (2009) J Pharm Biomed Anal 49:64–71
22. Ruta J, Zurlino D, Grivel C, Heinisch S, Veuthey JL, Guillarme D (2012) J Chromatogr A 1228:221–231
23. Guiochon G, Gritti F (2011) J Chromatogr A 1218:1915–1938
24. Kirkland JJ (1992) Anal Chem 64:1239–1245
25. Liekens A, Denayer J, Desmet G (2011) J Chromatogr A 1218:4406–4416
26. Olah E, Fekete S, Fekete J, Ganzler K (2010) J Chromatogr A 1217:3642–3653
27. Fanigliulo A, Cabooter D, Bellazzi G, Tramarin D, Allieri B, Rottigni A, Desmet G (2010) J Sep Sci 33:3655–3665
28. Staub A, Zurlino D, Rudaz S, Veuthey JL, Guillarme D (2011) J Chromatogr A 1218:8903–8914
29. Fekete S, Rudaz S, Fekete J, Guillarme D (2012) J Pharm Biomed Anal 70:158–168
30. Fekete S, Rudaz S, Veuthey JL, Guillarme D (2012) J Sep Sci. doi:10.1002/jssc.201200297
31. Snyder LR (1980) In: Horvath C (ed) Gradient elution in HPLC: advances and perspectives, vol. 1. Academic Press, New York
32. Snyder LR, Kirkland JJ, Glajch JL (1997) Practical HPLC method development, 2nd edn. John Wiley & Sons Inc., New York
33. Giddings JC (1967) Anal Chem 39:1027–1028
34. Horvath C, Lipsky SR (1967) Anal Chem 39:1893–1895
35. Neue UD (2005) J Chromatogr A 1079:153–161
36. Wang X, Stoll DR, Schellinger AP, Carr PW (2006) Anal Chem 78:3406–3416
37. Dolan JW, Snyder LR, Djordjevic NM, Hill DW, Waeghe TJ (1999) J Chromatogr A 857:1–20
38. Neue UD, Mazzeo JR (2001) J Sep Sci 24:921–929
39. Neue UD, Carmody JL, Cheng YF, Lu Z, Phoebe CH, Wheat TE (2001) Adv Chromatogr 41:93–136
40. Neue UD, Cheng YF, Lu Z (2006) In: Kromidas S (ed) HPLC made to measure: a practical handbook for optimization. Wiley-VCH, Weinheim
41. Schuster SA, Boyes BE, Wagner BM, Kirkland JJ (2012) J Chromatogr A 1228:232–241
42. Neue UD (2008) J Chromatogr A 1184:107–130
43. Wang X, Stoll DR, Carr PW, Schoenmakers PJ (2006) J Chromatogr A 1125:177–181
44. Zhang Y, Wang X, Mukherjee P, Petersson P (2009) J Chromatogr A 1216:4597–4605
45. Causon TJ, Hilder EF, Shellie RA, Haddad PR (2010) J Chromatogr A 1217:5063–5068
46. Ruta J, Guillarme D, Rudaz S, Veuthey JL (2010) J Sep Sci 33:2465–2477
47. Broeckhoven K, Cabooter D, Lynen F, Sandra P, Desmet G (2010) J Chromatogr A 1217:2787–2795
48. Broeckhoven K, Cabooter D, Eeltink S, Desmet G (2012) J Chromatogr A 1228:20–30
49. Bristow PA, Knox JH (1977) Chromatographia 10:279–289
50. Fekete S, Fekete J (2011) Talanta 84:416–423
51. Wang X, Barber WE, Carr PW (2006) J Chromatogr A 1107:139–151

52. McCalley DV (2006) Anal Chem 78:2532–2538
53. Fekete S, Berky R, Fekete J, Veuthey JL, Guillarme D (2012) J Chromatogr A 1252:90–103
54. Lundell N, Schreitmuller T (1999) Anal Biochem 266:31–47
55. Williams KR, Stone KL (1995) Methods Mol Biol 40:157–175
56. Yan B, Valliere-Douglass J, Brady L, Steen S, Han M, Pace D, Elliott S, Yates Z, Balland A, Wang W, Pettit D (2007) J Chromatogr A 1164:153–161
57. Kleemann G, Beierle J, Nichols A, Dillon T, Pipes G, Bondarenko P (2008) Anal Chem 80:2001–2009
58. Dillon TM, Bondarenko PV, Rehder DS, Pipes GD, Kleemann GR, Ricci MS (2006) J Chromatogr A 1120:112–120
59. Yang J, Wang S, Liu J, Raghani A (2007) J Chromatogr A 1156:174–182
60. Yan B, Eris T, Yates Z, Hong RW, Steen S, Kleemann G, Wang W, Liu JL (2009) J Chromatogr B 877:1613–1620